Brain cerebrospinal fluid flow

Douglas H. Kelley

Phys. Rev. Fluids **6**, 070501 — Published 23 July 2021

DOI: 10.1103/PhysRevFluids.6.070501

Brain cerebrospinal fluid flow

Douglas H. Kelley*

Department of Mechanical Engineering, University of Rochester,

Rochester, New York 14627, USA

Abstract

Cerebrospinal fluid flows around and into the brain, driven by intricate mechanisms, with profound implications for human health. According to the glymphatic hypothesis, in physiological conditions, cerebrospinal fluid flows primarily during sleep and serves to remove metabolic wastes like the amyloid-beta and tau proteins whose accumulation is believed to cause Alzheimer's disease. This paper reviews one research team's recent *in vivo* experiments and theoretical studies to better understand the fluid dynamics of brain cerebrospinal fluid flow. Driving mechanisms are considered, particularly arterial pulsation. Flow correlates closely with artery motion and changes when artery motion is manipulated. Though there are discrepancies between *in vivo* observations and predictions from simulations and theoretical studies of the mechanism, realistic boundary conditions bring closer agreement. Vessel shapes are considered, and have elongation that minimizes their hydraulic resistance, perhaps through evolutionary optimization. The pathological condition of stroke is considered. Much tissue damage after stroke is caused by swelling, and there is now strong evidence that early swelling is caused not by fluid from blood, as is commonly thought, but by cerebrospinal fluid. Finally, drug delivery is considered, and demonstrations show the glymphatic system could quickly deliver drugs across the blood-brain barrier. The paper closes with a discussion of future opportunities in the fast-changing field of brain fluid dynamics.

* d.h.kelley@rochester.edu

I. INTRODUCTION

The human body is 70% water, much of it flowing. Blood comes first to mind. Arteries, veins, and capillaries visit nearly every bit of human tissue, and the cardiovascular system is a primary transporter of nutrients, wastes, and fluid. But in the body, there is another, distinct fluid transport system. Capillaries in peripheral tissues leak, and much fluid escapes the cardiovascular system through the capillary walls, percolating through surrounding tissue and picking up cellular wastes via diffusion, before being gathered again by a separate set of fluid-carrying vessels: the lymph system. (Its fluid dynamics is the subject of an excellent recent review [1].) One-way valves in lymph vessels ensure that flow proceeds directionally, carried through a series of mergers into larger and larger lymph vessels on its way to rejoin the blood. Flow of lymph is driven partly by intrinsic pulsation of the vessels, many of which can contract spontaneously a few times per minute. Flow is also driven when we move our bodies, causing nearby muscles to squeeze lymph vessels and force fluid downstream. Failures of the lymph system can lead to severe swelling, known as lymphedema. The lymph system, however, does not extend into the brain. That fact has long been a puzzle, because the brain accounts for just 2% of human mass but 25% of glucose use, so its vigorous metabolic activity produces tremendous amounts of waste.

We are coming to understand that just as there are two distinct fluid transport systems in the body, there are also two distinct fluid transport systems in the brain. Direct evidence comes from injecting dye (tracer) into the brain and imaging its spread over time, as shown in Fig. 1. In this experiment, bovine serum albumin (BSA) dye was injected into the skull of a live, sedated mouse. Dye traveled to the base of the brain, then ascended around the edges and across the surface before diving into brain tissue. Dye apparently followed arteries closely, though it was dissolved in the water-like cerebrospinal fluid (CSF) in which the brain is immersed, not in blood. Dye did not spread uniformly across the skull, and it spread much faster than diffusion alone could have achieved (the diffusivity of BSA is about 7×10^{-11} m^2/s [2]), giving strong evidence that dye was being transported not only by diffusion but also by fluid flow — advection. Experiments with rats [3], pigs [4], and humans [5] have shown many of the same phenomena.

The brain, however, is a special place, and its fluid transport systems are not the same as those in peripheral tissue. Only in the last few years has it been discovered that lymph vessels

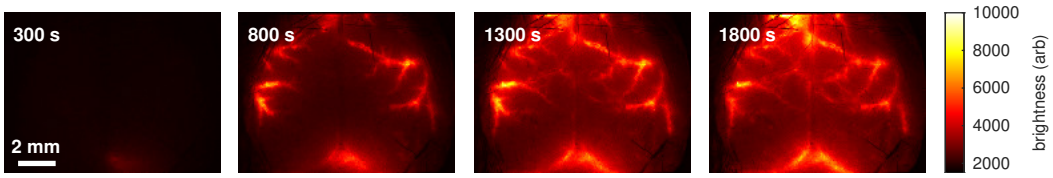

FIG. 1. Inflow of cerebrospinal fluid to the brain, visualized with dye. The brain of a live, anesthetized mouse is seen from above, imaged through the intact skull. Dye is transported much faster than diffusion alone could do, and does not spread uniformly, instead following pathways that nearly match the shapes of arteries (though the dye is not in arteries). Experiments like these give simple evidence that the brain has a fluid transport system distinct from the cardiovascular system — the glymphatic system. Transcranial imaging courtesy of H. Mestre and M. Nedergaard.

reach the skull at all [6–9]. Still, they visit only the edges, never penetrating into brain tissue. Rather, CSF seems to enter brain tissue by flowing along perivascular spaces (PVSs), annular regions that surround arteries. As arteries branch, PVSs do as well, eventually penetrating deep into brain tissue. From there, CSF percolates through the extracellular spaces around neurons and glia (and perhaps also along PVSs, which might be continuous from arteries to capillaries to veins [10]), finding its way to PVSs surrounding veins, or to nerve sheaths (annular regions that surround nerves), which carry it out of the brain and eventually to the lymph system. The idea of this brain-wide fluid transport pathway, and that its action is enabled by a particular membrane protein called aquaporin-4, is known as the "glymphatic hypothesis" and was first put forward in this form by Jeff Iliff, Maiken Nedergaard, and collaborators in 2012 [11], though earlier studies did find evidence for mass transport via flowing CSF and drew analogies to the lymph system [12–14]. The Nedergaard group also discovered that the glymphatic system is primarily active during sleep [15]. Excellent recent reviews give more background [16–20]. CSF in the brain is continuous with CSF in the spinal column and shares some flow characteristics; for more information, see e.g. [21–23].

The differences between the glymphatic system and the peripheral lymph system raise countless questions. Given that brain capillaries do not leak, but rather are sealed with tight junctions (part of the blood-brain barrier), what drives fluid to percolate through brain tissue? Without the one-way valves of lymph vessels, how is the fluid flow direction set? What fluid-dynamical mechanism regulates the observed sleep/wake variation of

glymphatic flow, which also depends on circadian rhythms [24]? Since neurodegenerative disorders like Alzheimer's disease correlate with unhealthy accumulation of normal brain metabolic wastes like amyloid-β and tau, are those disorders linked to poor glymphatic function? If so, could they be treated or prevented by manipulating the glymphatic system? Since pathological situations like stroke, cardiac arrest, and traumatic brain injury damage tissue largely through local swelling, might this fluid transport system be linked to those pathologies as well? If so, could clinical interventions altering glymphatic function during such pathological situations improve patient outcomes? Could the glymphatic system be leveraged to deliver drugs to the brain? These and related questions are important reasons for ongoing and expanded studies of the glymphatic fluid transport system.

II. EXPERIMENTAL METHODS

My colleagues and I seek to understand the glymphatic system through a combination of theory, simulation, and experiments. Much of our work is driven by *in vivo* observations done in the laboratories of Maiken Nedergaard, and in this paper, two sorts are discussed. Figure 2 summarizes both. In some experiments (including the one that produced Fig. 1), we perform transcranial imaging [25], in which we image the brain of a live mouse, from above, through the intact skull, which is thin enough to pass light. For flow visualization, we inject dye into the cisterna magna, a large fluid space ("cistern") at the back of the skull. The spatial resolution of transcranial imaging is relatively poor, and we get little information about the depth of the dye we see, but the wide field of view spans much of the brain cortex and allows direct observation of brain-wide phenomena.

In other experiments, we use two-photon imaging, in which we remove a patch of skull and replace it with a glass cranial window to allow sharper images. We keep the dura intact (and support it with a cranial window) to minimize perturbations to the intracranial pressure. Two-photon imaging leverages nonlinear optical phenomena to achieve much higher spatial resolution and allows us to image local regions in one, two, or three dimensions, to depths as great as a few hundred microns. The field of view, however, is much smaller than with transcranial imaging. In all measurements discussed in this paper, mice were sedated with ketamine-xylazine, which produces glymphatic function similar to natural sleep [26]. With two-photon imaging, as with transcranial imaging, we often inject dye into the cis-

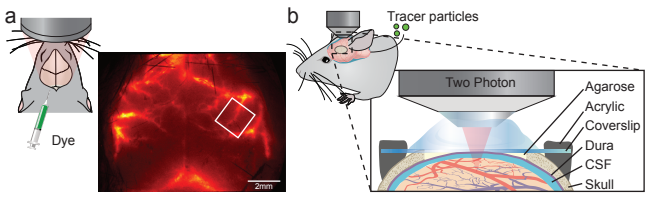

FIG. 2. Methods for imaging CSF flow in the brains of live mice. (a) Transcranial imaging uses an optical microscope with relatively low magnification to image the top surface of the brain, typically with scalp parted but skull intact. (b) Two-photon imaging uses a confocal, two-photon microscope, typically viewing a small region of tissue through a glass cranial window that has been installed in place of a patch of skull, while keeping the dura intact. The square overlaid on (a) indicates the approximate region we typically explore with two-photon imaging.

terna magna. On the other hand, we can measure flow more quantitatively if we instead inject tracer particles, typically 1-μm fluorescent polystyrene spheres, small enough and with buoyancy near enough to neutral that they follow fluid motions faithfully.

Figure 3 shows typical measurements made by tracking particles visualized via two-photon imaging. We use an automated, predictive algorithm for particle tracking that evolved from algorithms written for turbulence experiments [27, 28]. Examples of particle paths are shown in Fig. 3a. The observed particles traveled through the PVS surrounding a surface (pial) artery near the middle cerebral artery. Blood vessels are shown in gray for reference. By dividing the field of view into a grid of small regions and averaging all velocities measured in each, we can calculate the mean flow, as shown in Fig. 3b.

III. LAMINAR FLOW THROUGH OPEN SURFACE PERIVASCULAR SPACES

These velocity measurements reveal much about CSF flow in surface PVSs. Though some particles travel much faster, the overall mean speed is on the order of $U = 20$ μm/s. As shown, perivascular spaces are about $L = 40$ μm wide. Since CSF is essentially water — its protein content is lower than almost any other bodily fluid — we assume its viscosity and density to be that of water at 36.8°C: $\mu = 6.93 \times 10^{-4}$ Pa·s and $\rho = 995$ kg/m^3, respectively. Thus the Reynolds number is $\mathrm{Re} = UL\rho/\mu \sim 10^{-3}$, small enough that we expect the nonlinear term of the Navier-Stokes equation to be negligible, precluding turbulence. Deeper

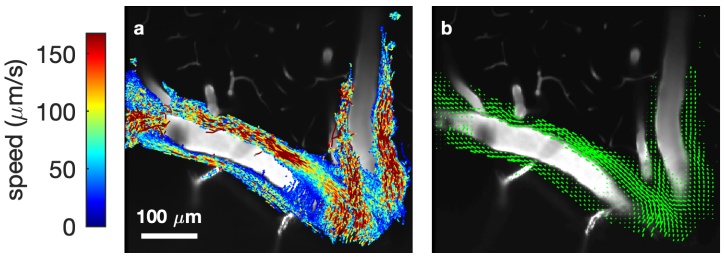

FIG. 3. Measuring cerebrospinal fluid flow in the brain of a live mouse. (a) Paths of tracer particles, colored according to their instantaneous speed, closely match fluid motion in the perivascular space. The background image shows nearby blood vessels. (b) The velocity, in many square regions, averaged over time. The measured velocities have typical characteristics of a laminar flow. Two-photon imaging and particle tracking courtesy of S. Holstein-Rønsbo, Y. Gan, and M. Nedergaard.

in the brain, flow is slower and spaces are smaller, again ruling out turbulent behaviors. These measurements (and similar measurements from many dozens of additional experiments we have performed) also show that CSF passes along PVSs in the direction parallel to blood flow, not anti-parallel, contrary to prior hypotheses and indirect evidence from fixed tissue [29]. Probably the discrepancy arose because the protocols for fixing tissue cause dramatic and atypical flows through the glymphatic system, which drive dye to places it does not visit *in vivo* [30].

Before starting experiments like these, my collaborators and many others speculated that brain PVSs might be filled with fibers and tissue, which would effectively constitute a porous medium. Then, we would expect CSF to flow much like groundwater through soil, with velocity profiles that are nearly uniform in space and consistent with Darcy's law. However, the velocities shown in Fig. 3 are evidently not uniform, instead varying from high speeds near the PVS centerline to near-zero speeds at the boundaries. Those characteristics are instead consistent with Poiseuille flow (pressure-driven laminar flow), suggesting that surface PVSs are open, not porous.

To test that hypothesis, my colleagues and I examined velocity profiles at multiple locations in multiple PVSs in multiple mice. Figure 4 shows one example. Averaging and interpolating measurements from particle tracking onto a cross-section, we constructed velocity profiles from our measurements. We compared them to the uniform profiles expected from Darcy flow (set to have the same mean speed as the measurements) and also to pro-

files calculated for Poiseuille flow. Calculating those profiles required approximating the cross-sectional shape of the PVS, which we knew only partly, because our measurements came from a plane approximately parallel to the PVS axis, not perpendicular. To make the approximation, we assumed the artery to be circular, assumed the outer boundary of the PVS to be elliptical, and determined the radius, semi-major axis, semi-minor axis, and eccentricity that produced a velocity profile that matched our data best. (Our choice of that shape will be explained below.) As with Darcy flow, we set the mean velocity to be the same as measured. As Fig. 4 shows, Poiseuille flow fits our data much better than Darcy flow, consistent with the hypothesis that PVSs are open, not porous. Going further, we examined the displacements of many tracer particles as they grew over time t, finding that their displacement scaled linearly with t, as expected for flow along an open space, not with $t^{1/2}$, as expected for flow through a porous medium. We concluded that surface PVSs are open. However, the penetrating PVSs that dive into the cortex may be filled with a porous medium, which would explain the fact that our tracer particles almost never pass from surface PVSs to penetrating PVSs, though dyes almost always do. More details are given in [31].

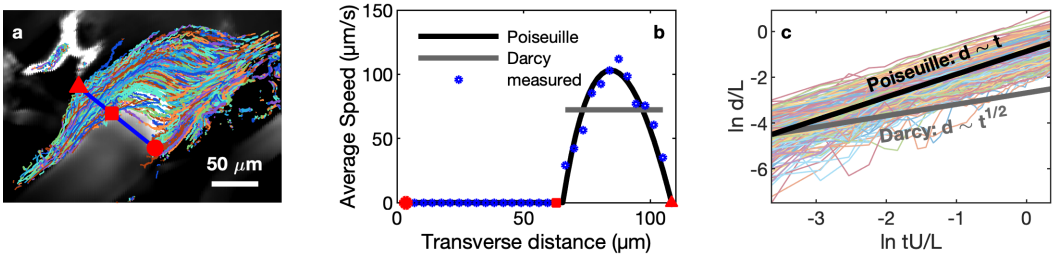

FIG. 4. Surface perivascular spaces are open, not filled with porous media. (a) Paths of tracer particles observed in a surface perivascular space via two-photon imaging. The thick blue line and red shapes mark one cross-section. (b) The measured velocity profile, along the cross-section marked in (a), does not match the velocity profile expected for Darcy flow in a porous medium, but closely matches the velocity profile expected for Poiseuille flow in an open space whose cross-section is fit to the measurements. (c) Particle displacements d increase linearly with time t, as expected for Poiseuille flow, not as the square root of time, as expected for Darcy flow. Here $L = 40$ μm and $U = 68$ m/s. Adapted from [31].

IV. THE ODD SHAPES OF PERIVASCULAR SPACES

Looking back again at Fig. 3, it is evident that in long parts of PVSs, particles tend to pass alongside the arteries, but rarely pass above or below. That observation is consistent with images of surface PVSs in mice [30, 32] and in humans [33], which show that their cross-sections are not concentric or circular, but eccentric and elongated (flattened). My colleague Jack Thomas became curious about the odd shapes, wondering how they might affect fluid flow. He devised a simple characterization, shown in Fig. 5, in which the inner boundary of the PVS is a circular artery of radius r_1, and the outer boundary is an elliptical wall with semimajor axis r_2 and semiminor axis r_3, whose center is offset from the artery center by $c\hat{\mathbf{x}} + d\hat{\mathbf{y}}$ in Cartesian coordinates (x, y, z). The flow through the PVS is governed by the momentum equation,

$$\rho\left(\frac{\partial \mathbf{u}}{\partial t} + (\mathbf{u}\cdot\nabla)\,\mathbf{u}\right) = -\nabla p + \mu\nabla^2\mathbf{u}, \tag{1}$$

where $\mathbf{u}$ is velocity and p is pressure. Assuming a straight vessel with uniform cross-section, and further assuming the flow to point purely in the $\hat{\mathbf{z}}$ direction, to be steady, and to be driven by a uniform pressure gradient $\partial p/\partial z$, Eq. 1 simplifies to

$$\frac{\partial^2 u_z}{\partial x^2} + \frac{\partial^2 u_z}{\partial y^2} = \frac{1}{\mu}\frac{\partial p}{\partial z}, \tag{2}$$

where $u_z = \mathbf{u}\cdot\hat{\mathbf{z}}$. Solving Eq. 2 numerically, with no-slip boundary conditions, for different shapes built with the simple characterization shows that elongation affects flow speed strongly (Fig. 5b). More specifically, for shapes lacking eccentricity ($c = d = 0$) and having the same area A, flow is slow when the elongation $(\alpha - \beta)/K$ (where $\alpha = r_2/r_1, \beta = r_3/r_1$, and $K = A\pi^{-1}r_1^{-2}$) is zero, much faster when the elongation is moderate, and slow again when the elongation is large. That variation is consistent with expectations for Poiseuille flow: only with moderate elongation is any part of the region far enough from the no-slip walls to allow fast flow.

Intrigued, my colleagues and I wondered how real PVS shapes might compare. We fit ellipses and circles to three *in vivo* images of of PVSs, determining the values of r_1, r_2, r_3, c and d for each. Then, we calculated the normalized hydraulic resistance $r_1^4\mathcal{R}/\mu$ of many shapes having varying elongation $(\alpha - \beta)/K$ but identical r_1, c, d, and A. Here $\mathcal{R}$, the hydraulic resistance per unit length, is the proportionality constant linking the pressure

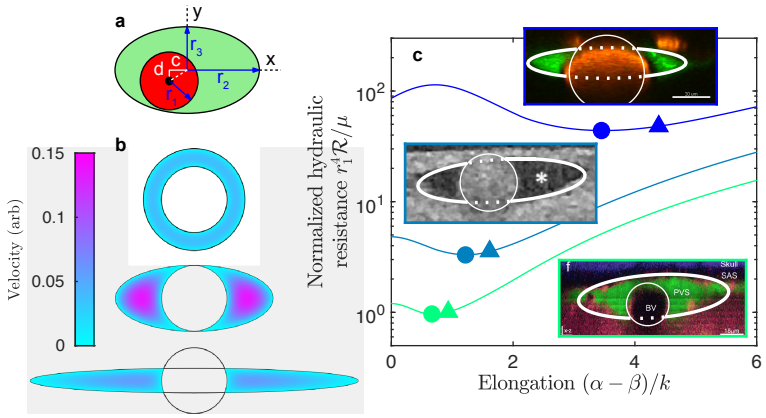

FIG. 5. Surface perivascular spaces have nearly optimal shapes. (a) A surface perivascular space can be simply characterized as the region between a circular artery and an elliptical, eccentric outer wall. (b) Flow in vessels with cross-sectional shapes of this sort is fastest when elongation is neither too great nor too little. (c) Using the measured area, artery radius, and eccentricity of three different previously published perivascular spaces, we varied the elongation, calculating the resulting hydraulic resistance. We found a single minimum in each case. The calculated resistances of the observed spaces (triangles) nearly match the minima (circles). Adapted from [34].

gradient to the volume flow rate; as its name implies, lower resistance permits faster flow with smaller pressure gradients. In each case, we found a unique value of the elongation that minimized the normalized hydraulic resistance. In each case, the shape observed *in vivo* had nearly the same elongation, with nearly the minimum resistance, as Fig. 5 shows. Perhaps, then, these odd shapes arose evolutionarily because they minimize the hydraulic resistance of surface PVSs, therefore reducing the energy required to pump CSF and spreading CSF more uniformly across the brain surface before it enters the cortex. Going further, we also examined penetrating PVSs, which typically have little elongation ($r_2 = r_3$) but high eccentricity, finding that their eccentricity likewise serves to reduce hydraulic resistance (not shown). Though these flows are in fact not steady (as discussed below), their Womersley number is low enough that the actual hydraulic resistance closely matches the value for the steady case. More details are given in [34]. The best-fit shapes we used to produce Fig. 4 and similar analyses [31] were motivated by these findings; they were ellipses of optimal elongation.

V. ARTERIAL PULSATION AND FLUID FLOW

Close examination of the particle tracks in Fig. 3 shows that their speeds vary quasi-periodically over time; the flow pulses. That pulsation is present in virtually every experiment we have done with healthy animals, and as with any fluid-dynamical phenomenon, determining its frequency might give hints about the underlying mechanisms. To do so, we calculated the instantaneous root-mean-square velocity $v_{\mathrm{rms}} = \langle |\mathbf{u}|^2 \rangle^{1/2}$, where brackets $\langle \cdot \rangle$ signify averaging over space. Figure 6a shows v_{rms} in one experiment, along with simultaneous measurements of the heartbeat via electrocardiogram (ECG), as well as respiration. Both the heartbeat and respiration are quasi-periodic signals that have strong influence throughout the body, so one naturally wonders whether they might play a key role in glymphatic function. The measurements reveal that CSF flow pulses in synchrony with the heart, not with respiration, and additional measurements with more mice have shown the same.

Flow pulsing in synchrony with the heart is predicted by a prior hypothesis for pumping CSF through PVSs. Each time the heart beats, a traveling wave propagates down the muscular artery walls, and that wave might pump CSF via a peristalsis-like mechanism known as perivascular pumping [35, 36]. Exploring further, my colleagues and I used two-photon imaging to measure the transverse velocity of artery walls at multiple locations along PVSs and in multiple animals, while simultaneously measuring ECG signals. Then we phase-averaged the artery wall velocity over the cardiac cycle. That is, for each individual wall velocity measurement, the corresponding phase (0 to 2π) of the cardiac cycle at the same moment was determined. Then, we gathered velocity measurements of similar phase and averaged them. We also phase-averaged $\Delta v_{\mathrm{rms}} = v_{\mathrm{rms}} - \overline{v_{\mathrm{rms}}}$, the fluctuating component of v_{rms} (where the over-line $\bar{\cdot}$ signifies averaging over time). As Fig. 6b shows, the artery wall velocity and fluid velocity are remarkably similar, with peaks that align closely, further supporting the peristaltic pumping hypothesis.

Correlation is not causality, however. If CSF is pumped by artery wall motion, we reasoned, then altering the wall motion should alter CSF flow. To test, we gave mice a drug to raise their blood pressure. High blood pressure causes artery walls to stiffen, necessary for maintaining constant vascular volume under increased pressure. Stiff muscle tissue has different mechanical properties than relaxed muscle tissue (higher shear modulus), such

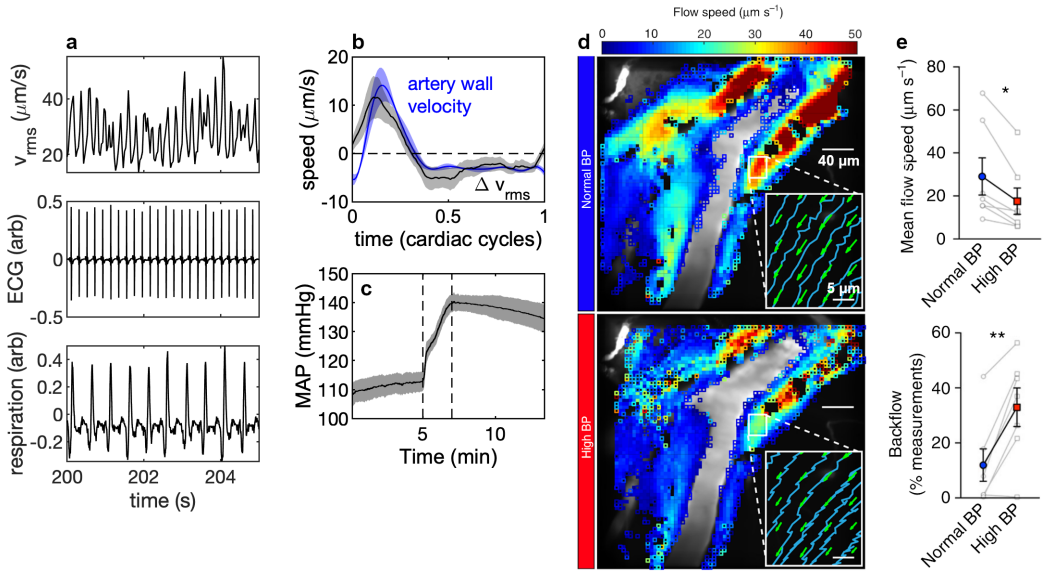

FIG. 6. Arterial pulsation is a primary driver of flow in perivascular spaces. (a) The instantaneous root-mean-square flow velocity pulses in synchrony with the ECG signal (which indicates cardiac activity), not with respiration. (b) Artery wall velocity closely matches fluctuations in root-mean-square flow velocity. (c) The drug angiotensin II raises the mean arterial pressure (MAP), presumably stiffening artery walls. $N = 4$ mice. (d) With high blood pressure, time-averaged flow in perivascular spaces (measured using two-photon imaging) is slower, and particle paths (insets) often show upstream motion. (e) Inducing high blood pressure (BP) causes a decrease in mean flow speed and an increase in the backflow fraction; both effects are statistically significant. $N = 7$ mice. Adapted from [30].

that we expect waves propagate more quickly. Thus, altering blood pressure gave us a way to modulate artery wall motion, to determine if CSF flow would change accordingly. As Fig. 6c shows, the drug, angiotensin II, raised blood pressure by 30 mmHg in 2 minutes. Its quick action allowed us to measure CSF flow in the same animals, both before and after raising blood pressure, eliminating animal-to-animal variations that might confound analysis. The results are shown in Fig. 6d–e. With high blood pressure, the mean flow is significantly slower than without. Moreover, with high blood pressure, flow pulsation results in backflow — that is, instantaneous motion opposite the mean flow direction — significantly more often than without. Our results show that altering wall motion does indeed alter CSF flow, supporting the hypothesis that arterial pulsation is a primary driver of CSF in PVSs

under healthy conditions. More details are given in [30]. High blood pressure has been found to impede glymphatic transport in rats [37] and is a known risk factor for Alzheimer's disease in humans, perhaps because it reduces CSF flow in PVSs.

VI. MORE ABOUT ARTERIAL PULSATION: COMPARING TO SIMULATION AND THEORY

Though we have observed the flow characteristics described above in many dozens of experiments, and though the one other study employing *in vivo* particle tracking found similar speeds and pulsations [33], when pondering how glymphatic flow is driven, many mysteries remain. In fact, theoretical models and simulations have often disagreed with those experimental observations. For example, a recent simulation by Kedarasetti *et al.* [38] considered a domain with a cross-sectional shape like those sketched in Fig. 5, then imposed traveling-wave pulsations on the artery wall, with the same waveform we measured *in vivo* (Fig. 6b). The domain was one wavelength long and had $p = 0$ end boundary conditions. The resulting flow had centerline velocity 102 μm/s, in good agreement with Fig. 3 and other *in vivo* measurements. However, the simulation results showed flow peaks that did not have the same phase as the wall velocity peaks, as we would expect from Fig. 6b; rather, there was a $\sim 30^\circ$ phase difference. An even more striking discrepancy appeared when considering the ratio of mean flow to fluctuation, which was about 0.5 *in vivo* but about 300 in the simulation. Though the results of Kedarasetti *et al.* disagree with *in vivo* measurements, they broadly agree with other simulations [39, 40] and with theoretical predictions using lubrication theory [41, 42]. Many studies of peristaltic pumping using realistic parameters have predicted mean flows of the same order of magnitude as those observed *in vivo*, but flow peaks do not align with wall peaks, and velocity fluctuations are far faster than the mean flow. Given these discrepancies, is peristaltic pumping really a primary driver?

To explain the discrepancies, some have hypothesized that the flows observed *in vivo* are artifacts driven by the injection of tracer particles into the cisterna magna [38, 43–49]. My colleagues and I previously showed that the observed flows persisted far longer than the injection duration, without exhibiting the exponential decay over time that would be expected in artefactual flow driven by the inflation and subsequent relaxation of a compliant membrane [30]. Still, to double-check that the observed flows are not artifacts, we revisited

the question. Specifically, we performed a series of experiments as sketched in Fig. 7a. In each, we injected tracer particles suspended in fluid as usual, but unlike in prior experiments, we simultaneously withdrew an equal amount of fluid from the cisterna magna. With the volume of fluid in the skull remaining unchanged, we expected the intracranial pressure to hold steady, and it did, as Fig. 7 shows. Using the same protocols as in prior experiments, we performed particle tracking, then calculated v_{rms}, the mean velocity, and the backflow fraction. All were statistically indistinguishable from prior experiments in which only a single syringe was used. We concluded that CSF flows observed in surface PVSs are not injection artifacts. More details are given in [50].

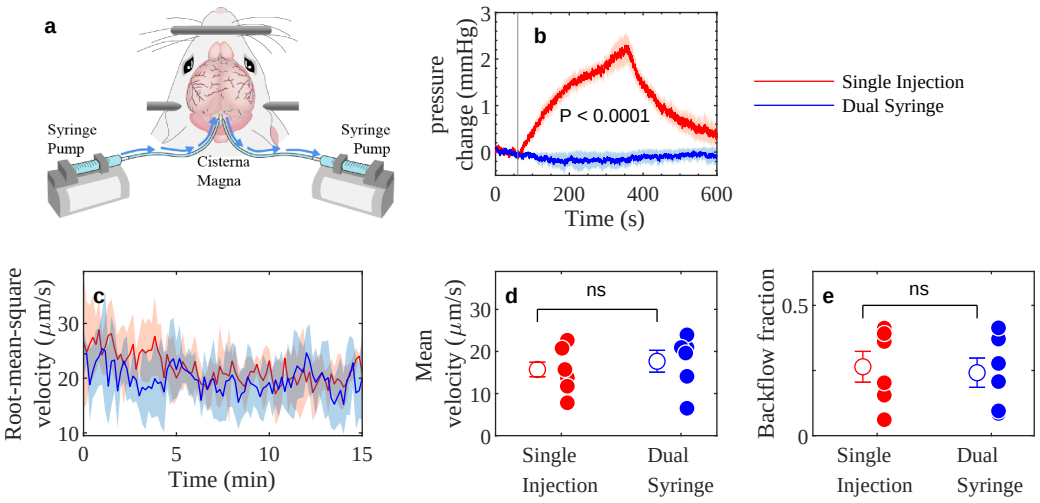

FIG. 7. Dual-syringe experiments demonstrate that observed flows are not injection artifacts. (a) While injecting a solution of tracer particles with one pump, we withdrew an equal amount of fluid with another. (b) Simultaneous withdrawal and injection eliminates the increase in intracranial pressure observed when injecting without withdrawing. (c) Root-mean-square fluid velocity in the middle cerebral artery is similar in either sort of experiment. Shaded regions indicate standard error of the mean, from 6 single-injection experiments and 6 dual-syringe experiments. (d–e) Neither the mean velocity, nor the fraction of time during which the flow direction reverses, differ significantly from one sort of experiment to the other. Error bars indicate mean ± standard error. Adapted from [50].

An alternative hypothesis for explaining the discrepancies between theory, simulation, and *in vivo* observations involves boundary conditions. Simulations and theoretical treatments

of perivascular pumping have each considered a segment of PVS, either setting $p = 0$ at the ends or applying periodic boundary conditions to the ends. That is, segments of PVS have been modeled in isolation. Isolating them is entirely reasonable, both because the rest of the glymphatic pathway has been characterized in far less detail, and because the glymphatic system is so large and complicated that direct numerical simulation of the whole system would be impractically expensive. Still, it is natural to wonder how model predictions might be affected by coupling the models to the rest of the glymphatic pathway. To start to answer that question, we characterize the pathway with two parameters, its hydraulic resistance R and compliance C, as sketched in Fig. 8a. If p is the pressure across the system and q is the volume flow rate through the system, then the resistance $R = p/q$ quantifies viscous resistance to flow, and the compliance $C = q\,/(\partial p/\partial t)$ quantifies elastic effects. A high compliance implies that vessel walls can stretch substantially, temporarily making more room for fluid in the system, before contracting again later. (Hydraulic resistance is analogous to electrical resistance, and compliance is analogous to electrical capacitance.) Considering the fluid circuit sketched in Fig. 8a and asserting conservation of mass and energy leads to a relationship between the flow rate q_0 in the PVS and the flow rate q_1 downstream:

$$\frac{\partial q_1}{\partial t} + \frac{q_1}{RC} = \frac{q_0}{RC}. \tag{3}$$

This expression allows us to estimate the flow rate q_1 that would be observed when a PVS is coupled to the rest of the glymphatic system, if we know the flow rate when the PVS is isolated (q_0), as well as R and C.

We determined that $R = 1.097 \pm 0.09$ mmHg/(μL/min) and $C = 1.798 \pm 0.19$ μL/mmHg via bolus-injection experiments, in which we rapidly injected large amounts of fluid into the skulls of live mice, then measured how the pressure decayed. Then, we defined the uncoupled flow rate q_0 to be the product of the centerline velocity predicted by Kedarasetti *et al.* and the cross-sectional area of their simulation domain. (The centerline velocity is higher than the mean velocity, so we over-estimated the volume flow rate by a small, constant factor.) Using Eq. 3, we calculated the coupled flow rate q_1, which is shown in Fig. 8. The mean velocity remained unchanged and continued to match observations reasonably well. The fluctuations in q_1 were much smaller than in q_0, and smaller than the mean, consistent with *in vivo* observations. During each cardiac cycle, the peak of q_1 aligned closely with the peak wall velocity (compare Fig. 8c to Fig. 6b). In fact, the q_1 waveform closely resembles

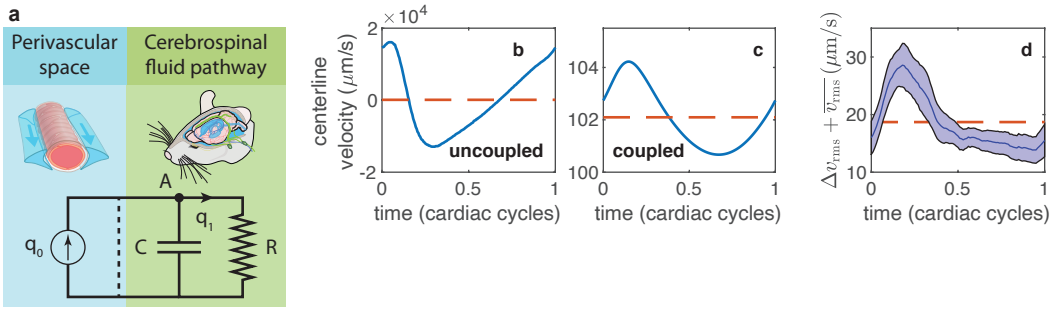

FIG. 8. Realistic end boundary conditions help reconcile results from experiments and simulations. (a) Simulating perivascular spaces with periodic or zero-pressure end boundary conditions predicts the flow in isolation (circuit closed by dashed line); resistance and compliance at the boundaries can approximate the effects of coupling to the rest of the flow pathway (larger circuit). (b) The simulated centerline velocity from Kedarasetti *et al.* [38] exhibits much larger velocity fluctuations than *in vivo* measurements, as well as a shifted velocity peak (compare to Fig. 6b). (c) The centerline velocity calculated from the Kedarasetti *et al.* results, using Eq. 3 to model coupling to the rest of the glymphatic system, exhibits much smaller velocity fluctuations and a velocity peak that occurs later in the cardiac cycle. (d) Flow velocities measured *in vivo* exhibit fluctuations, peak location, and overall shape that resemble the coupled prediction. Adapted from [51].

the experimental waveform (Fig. 8d. Thus, discrepancies between this simulation and *in vivo* observations were largely resolved by coupling the simulation to simple but realistic end boundary conditions. We performed similar calculations using two predictions from lubrication theory [41, 42], again finding that realistic end boundary conditions brought closer agreement with *in vivo* observations. More details are given in [51]. My colleagues and I believe that these finding strengthen the case for peristaltic pumping as a primary driver of CSF flow through PVSs in healthy conditions. That said, these simulations and lubrication theory models considered domains with lengths equal to the wavelength, but real PVSs are much shorter. Arterial pulsation seems to produce significantly different flows in shorter domains [40], so further investigation is warranted.

VII. PATHOLOGICAL CONDITIONS: STROKE

The glymphatic system is likely to play important roles in unhealthy, pathological situations as well. Strokes, for example, harm millions of people every year. Strokes damage brain tissue, often irreparably, and much of the damage is caused by severe swelling. That swelling, of course, occurs when fluid moves into the tissue, so my colleagues wondered if the glymphatic system, being a fluid transport system, might play a role.

A stroke occurs when a blood vessel in the brain is blocked, depriving nearby tissue of oxygen and energy. Neurons are then unable to maintain the unstable ion gradients which make them function; they release large numbers of ions into fluid in the extracellular space. Those ions make it far more difficult for neighboring neurons to maintain their own unstable gradients, so they, in turn, release ions. The result is a chain reaction — more specifically, a reaction-diffusion wave — known in the medical literature as spreading depolarization. It spreads across some or all of the brain, and its propagation is followed by a drastic inrush of fluid to the cells, causing swelling and possibly damage. This series of events during stroke is well known, and textbooks typically explain that the fluid which causes swelling comes from blood. At first, that seems reasonable, because stroke is known to open the blood-brain barrier by loosening the tight junctions in capillary walls. But swelling can be observed much sooner than the blood-brain barrier opens, suggesting another fluid source might also come into play.

To explore, my colleague Ting Du developed a protocol called middle cerebral artery obstruction (MCAO), which induces stroke in mice via injection of a sphere into the middle cerebral artery, as shown in Fig. 9a. She and others performed a series of experiments using Glt1-GCAMP7 mice that had been genetically modified such that their brain tissue fluoresces when neurons fire (when calcium ions are active), making spreading depolarization visible. Using two-color transcranial imaging and injecting dye into the cisterna magna as usual, we saw that the spreading depolarization wave was followed by an inrush of fluid — CSF, not blood — as shown in Fig. 9b. To quantify, we used front tracking, an automated method my team had previously invented for studying reactive mixing via advection, reaction, and diffusion [52, 53]. Front tracking works by finding the fronts (9c) that separate bright from dark regions in each frame of a movie, then calculating the local front velocity throughout space and time by measuring (locally perpendicular) front displacements from

frame to frame. Front tracking showed that CSF inflow followed spreading depolarization (Fig. 9d) and that the CSF inflow speed increased significantly after the spreading depolarization wave passed.

Wondering what mechanism might drive such a violent inrush of CSF, we looked closer at the PVSs where CSF enters the brain. Using two-photon imaging in line-scan mode to examine PVSs and arteries, we found that arteries constricted after the spreading depolarization front passed, leaving more space in the surrounding PVS. That space was then filled with CSF, as shown in Fig. 9f. As many segments of many arteries constricted, it seemed, large amounts of CSF were drawn from the space around the brain, causing violent inrush. Particle tracking in surface PVSs supported that idea, as shown in Fig. 9g. Before the wave passed, the flow had a mean speed similar to prior observations (compare to the upper panel of Fig. 6d), but after the wave passed, the flow was much faster. Moreover, the flow was pulsatile before the wave passed, but not after, consistent with the fact that a blocked artery does not propagate blood or arterial pulsations.

My colleagues performed additional analyses, including developing a mathematical model for fluid inrush driven by arterial constriction, using radioactive dyes to verify that fluid came not from blood but from CSF, imaging whole-brain swelling over time using MRI, and measuring brain mass over time to quantify fluid uptake. More details are given in [54]. Our findings strongly support the idea that swelling in the first few minutes after stroke is caused not by blood but by CSF. That conclusion has important clinical implications: manipulating the glymphatic system in the first few minutes after stroke might reduce tissue damage and improve patient outcomes. In ongoing work, we are also exploring the role of the glymphatic system in two other pathological situations in which swelling causes tissue damage: cardiac arrest and traumatic brain injury.

VIII. DRUG DELIVERY

Another topic where the glymphatic system may have important clinical implications is drug delivery. Because the blood-brain barrier allows few molecules to pass between blood and brain, drugs ingested or injected elsewhere in the body typically reach the brain only in tiny concentrations. Flowing CSF, however, transports fluid through brain tissue itself, without barriers or separation. Thus, it is natural to wonder whether drugs might be

delivered via the glymphatic system. Successful delivery would require some control of the system; when giving drugs, doctors would want to promote glymphatic flow. My colleague Maiken Nedergaard had the great idea to do it by altering brain osmolality. We injected a high-concentration solution of a common sugar (mannitol) into live mice, then injected dye into the cisterna magna, as a surrogate for a hypothesized drug. We characterized CSF motion via transcranial imaging, and the results are shown in Fig. 10.

Dye entered perivascular spaces and brain tissue much more quickly, and in greater quantities, in mice that had received the sugar solution than in those that instead received an osmotically neutral NaCl solution. In a separate set of experiments (not shown), we also demonstrated that high-concentration salt solution (hypertonic saline) works, too, and that even in awake animals, osmotic manipulations can increase CSF inflow beyond its usual rate during sleep. Details are given in [25].

IX. OUTLOOK

As human knowledge of brain fluid dynamics advances rapidly, new questions and new implications arise just as rapidly.

For example, my collaborators and I present results about surface PVSs more than the rest of the glymphatic system not because they are our sole interest, but because they are easier to image, making their flows easier to quantify. Flows through penetrating PVSs, brain tissue, venous PVSs, and nerve sheaths all deserve deeper study. Learning more about connections from the glymphatic system to the lymphatic system would also be fundamentally interesting and have potentially significant clinical implications. Moreover, the lymph system plays key roles in the body's immune responses. White blood cells frequently travel along lymph vessels, and antigen-containing fluid is swept into lymph nodes, where it is filtered and where more immune cells take action. The glymphatic system may likewise play important roles in immune response; further study is needed.

This paper has discussed a first step toward understanding how PVSs interact with the rest of the glymphatic system, which my colleagues and I characterized using one global resistance and one global capacitance. A much more nuanced understanding of the interactions of different parts of the glymphatic system, and its overall dynamics, could be gleaned from a global hydraulic network model, in which the resistances of multiple components of

the system are estimated separately and connected to make a large fluid circuit. Two such models were published fairly recently [55, 56], but knowledge of the glymphatic system is advancing so quickly that updates would be useful. My colleagues and I plan to publish a hydraulic network model soon.

The pathway of CSF flow is not as simple as a global, branching tree. Insight comes from arteries and veins on the brain surface, many of which share looped, direct connections that do not pass through brain tissue (see, e.g., [57]). Though loops make the network less efficient for fluid transport, they also make it more robust to failure, a key feature for the brain. PVSs may loop as well. Moreover, much CSF seems to bypass PVSs altogether, flowing directly from the cisterna magna to skull exit routes in the spine, nose, and neck, especially during wakefulness [24, 58, 59]. Understanding the drivers of those flows and the (perhaps valve-like) mechanisms that set CSF pathways is a fruitful topic of future study.

The flow of CSF in the brain is tightly coupled to the flow of blood in the brain. CSF in PVSs shares a moving boundary with blood in arteries: the artery wall. Moreover, the rigidity of the skull keeps its volume essentially constant, so that an inflow of blood must always be compensated by an outflow of some other fluid, most likely CSF. Blood flow to brain tissue varies locally and globally for many reasons, including the "slow waves" of neural activity that propagate across the brain during deep (NREM) sleep [26, 60]. Understanding the mechanisms that couple CSF flow, blood flow, and neural activity could have profound clinical implications.

Finally, though this paper has discussed experiments only in mice, our motivation is human health, so adding to the relatively small number of existing studies of CSF flow in human brains would be valuable. However, new methods are needed. Invasive methods like cranial windows or injection of dye and particles are almost never done in humans, for obvious reasons. Developing non-invasive methods for measuring fluid flow, one of which has been recently published [3, 61], will be important.

ACKNOWLEDGMENTS

The author is grateful for extensive collaboration with M. Nedergaard, J. H. Thomas, and J. Tithof; for previously unpublished data from H. Mestre, S. Holstein-Rønsbo, J. Tithof, Y. Gan, and M. Nedergaard; and for expert illustration by D. Xue. This work was supported by

the NIH/National Institute of Aging (grant RF1AG057575) and by the U. S. Army Research Office (grant MURI W911NF1910280).

---

[1] James E Moore Jr and Christopher D Bertram, "Lymphatic System Flows," Annu. Rev. Fluid Mech. **50**, 459–482 (2018).

[2] Adolfas K Gaigalas, Joseph B Hubbard, M McCurley, and Sam Woo, "Diffusion of bovine serum albumin in aqueous solutions," The Journal of Physical Chemistry **96**, 2355–2359 (1992).

[3] Vadim Ratner, Yi Gao, Hedok Lee, Rena Elkin, Maiken Nedergaard, Helene Benveniste, and Allen Tannenbaum, "Cerebrospinal and interstitial fluid transport via the glymphatic pathway modeled by optimal mass transport," NeuroImage **152**, 530–537 (2017).

[4] Nicholas Burdon Bèchet, Nagesh C Shanbhag, and Iben Lundgaard, "Glymphatic pathways in the gyrencephalic brain," J Cerebr Blood F Met , 0271678X21996175 (2021).

[5] Per Kristian Eide, Vegard Vinje, Are Hugo Pripp, Kent-André Mardal, and Geir Ringstad, "Sleep deprivation impairs molecular clearance from the human brain," Brain **144**, 863–874 (2021).

[6] Antoine Louveau, Igor Smirnov, Timothy J Keyes, Jacob D Eccles, Sherin J Rouhani, J David Peske, Noel C Derecki, David Castle, James W Mandell, Kevin S Lee, Tajie H Harris, and Jonathan Kipnis, "Structural and functional features of central nervous system lymphatic vessels," Nature **523**, 337–341 (2015).

[7] Aleksanteri Aspelund, Salli Antila, Steven T Proulx, Tine Veronica Karlsen, Sinem Karaman, Michael Detmar, Helge Wiig, and Kari Alitalo, "A dural lymphatic vascular system that drains brain interstitial fluid and macromolecules," J Exp Med **212**, 991–999 (2015).

[8] Sandro Mesquita, Antoine Louveau, Andrea Vaccari, Igor Smirnov, R Chase Cornelison, Kathryn M Kingsmore, Christian Contarino, Suna Onengut-Gumuscu, Emily Farber, Daniel Raper, Kenneth E Viar, Romie D Powell, Wendy Baker, Nisha Dabhi, Robin Bai, Rui Cao, Song Hu, Stephen S Rich, Jennifer M Munson, M Beatriz Lopes, Christopher C Overall, Scott T Acton, and Jonathan Kipnis, "Functional aspects of meningeal lymphatics in ageing and Alzheimer's disease," Nature , 1–32 (2018).

[9] Ji Hoon Ahn, Hyunsoo Cho, Jun-Hee Kim, Shin Heun Kim, Je-Seok Ham, Intae Park, Sang Heon Suh, Seon Pyo Hong, Joo-Hye Song, Young-Kwon Hong, Yong Jeong, Sung-Hong Park, and Gou Young Koh, "Meningeal lymphatic vessels at the skull base drain cerebrospinal fluid," Nature , 1–29 (2019).

[10] Melanie-Jane Hannocks, Michelle E Pizzo, Jula Huppert, Tushar Deshpande, N Joan Abbott, Robert G Thorne, and Lydia Sorokin, "Molecular characterization of perivascular drainage pathways in the murine brain," J Cerebr Blood F Met **38**, 669–686 (2018).

[11] J J Iliff, M Wang, Yang Liao, B A Plog, W Peng, G A Gundersen, H Benveniste, G E Vates, R Deane, S A Goldman, E A Nagelhus, and M Nedergaard, "A Paravascular Pathway Facilitates CSF Flow Through the Brain Parenchyma and the Clearance of Interstitial Solutes, Including Amyloid ," Science Translational Medicine **4**, 147ra111–147ra111 (2012).

[12] HF Cserr, DN Cooper, PK Suri, and CS Patlak, "Efflux of radiolabeled polyethylene glycols and albumin from rat brain," American Journal of Physiology-Renal Physiology **240**, F319–F328 (1981).

[13] Marshall L Rennels, Thomas F Gregory, Otis R Blaumanis, Katsukuni Fujimoto, and Patricia A Grady, "Evidence for a 'Paravascular' fluid circulation in the mammalian central nervous system, provided by the rapid distribution of tracer protein throughout the brain from the subarachnoid space," Brain Research **326**, 47–63 (1985).

[14] Takao Ichimura, P A Fraser, and H F Cserr, "Distribution of extracellular tracers in perivascular spaces of the rat brain," Brain Research **545**, 103–113 (1991).

[15] Lulu Xie, Hongyi Kang, Qiwu Xu, Michael J Chen, Yonghong Liao, Meenakshisundaram Thiyagarajan, John O'Donnell, Daniel J Christensen, Charles Nicholson, Jeffrey J Iliff, Takahiro Takano, Rashid Deane, and Maiken Nedergaard, "Sleep Drives Metabolite Clearance from the Adult Brain," Science **342**, 373–377 (2013).

[16] Helene Benveniste, "The Brain's Waste-Removal System," Cerebrum **2018**, cer–09–18 (2018).

[17] John H Thomas, "Fluid dynamics of cerebrospinal fluid flow in perivascular spaces," J. R. Soc. Interface **16**, 20190572–11 (2019).

[18] Lori A Ray and Jeffrey J Heys, "Fluid Flow and Mass Transport in Brain Tissue," Fluids **4**, 196–33 (2019).

[19] Maiken Nedergaard and Steven A Goldman, "Glymphatic failure as a final common pathway to dementia," Science **370**, 50 (2020).

[20] Martin Kaag Rasmussen, Humberto Mestre, and Maiken Nedergaard, "Fluid transport in the brain," Physiological Reviews **0**, null (0).

[21] Andreas A Linninger, Kevin Tangen, Chih-Yang Hsu, and David Frim, "Cerebrospinal Fluid Mechanics and Its Coupling to Cerebrovascular Dynamics," Annu. Rev. Fluid Mech. **48**, 219–257 (2016).

[22] J J Lawrence, W Coenen, A L Sánchez, G Pawlak, C Martínez-Bazán, V Haughton, and J C Lasheras, "On the dispersion of a drug delivered intrathecally in the spinal canal," J. Fluid Mech. **861**, 679–720 (2018).

[23] A L Sánchez, C Martínez-Bazán, C Gutiérrez-Montes, E Criado-Hidalgo, G Pawlak, W Bradley, V Haughton, and J C Lasheras, "On the bulk motion of the cerebrospinal fluid in the spinal canal," J. Fluid Mech. **841**, 203–227 (2018).

[24] Lauren M Hablitz, Virginia Plá, Michael Giannetto, Hanna S Vinitsky, Frederik Filip Stæger, Tanner Metcalfe, Rebecca Nguyen, Abdellatif Benrais, and Maiken Nedergaard, "Circadian control of brain glymphatic and lymphatic fluid flow," Nature communications **11**, 1–11 (2020).

[25] Benjamin A Plog, H Mestre, Genaro E Olveda, Amanda M Sweeney, H Mark Kenney, Alexander Cove, Kosha Y Dholakia, J Tithof, T D Nevins, Iben Lundgaard, Ting Du, D H Kelley, and Maiken Nedergaard, "Transcranial optical imaging reveals a pathway for optimizing the delivery of immunotherapeutics to the brain," JCI Insight **3**, 1188–16 (2018).

[26] Lauren M Hablitz, Hanna S Vinitsky, Qian Sun, Frederik Filip Stæger, Björn Sigurdsson, Kristian N Mortensen, Tuomas O Lilius, and Maiken Nedergaard, "Increased glymphatic influx is correlated with high EEG delta power and low heart rate in mice under anesthesia," Sci Adv **5**, eaav5447 (2019).

[27] N T Ouellette, H Xu, and E Bodenschatz, "A quantitative study of three-dimensional Lagrangian particle tracking algorithms," Exp. Fluids **40**, 301–313 (2006).

[28] D H Kelley and N T Ouellette, "Using particle tracking to measure flow instabilities in an undergraduate laboratory experiment," Am. J. Phys. **79**, 267–273 (2011).

[29] Jenna M Tarasoff-Conway, Roxana O Carare, Ricardo S Osorio, Lidia Glodzik, Tracy Butler, Els Fieremans, Leon Axel, Henry Rusinek, Charles Nicholson, Berislav V Zlokovic, Blas Frangione, Kaj Blennow, Joël Ménard, Henrik Zetterberg, Thomas Wisniewski, and Mony J de Leon, "Clearance systems in the brain—implications for Alzheimer disease," Nature Reviews Neurology **11**, 457–470 (2015).

[30] H Mestre, J Tithof, Ting Du, Wei Song, Weiguo Peng, Amanda M Sweeney, Genaro Olveda, John H Thomas, Maiken Nedergaard, and D H Kelley, "Flow of cerebrospinal fluid is driven by arterial pulsations and is reduced in hypertension," Nat. Commun. **9**, 4878 (2018).

[31] Fatima Min Rivas, Jia Liu, B C Martell, Ting Du, H Mestre, Maiken Nedergaard, J Tithof, John H Thomas, and D H Kelley, "Surface periarterial spaces of the mouse brain are open, not porous," J. R. Soc. Interface **17**, 20200593 (2020).

[32] Aaron J Schain, Agustin Melo-Carrillo, Andrew M Strassman, and Rami Burstein, "Cortical Spreading Depression Closes Paravascular Space and Impairs Glymphatic Flow: Implications for Migraine Headache," J Neurosci **37**, 2904–2915 (2017).

[33] Beatrice Bedussi, Mitra Almasian, Judith de Vos, Ed VanBavel, and Erik NTP Bakker, "Paravascular spaces at the brain surface: Low resistance pathways for cerebrospinal fluid flow," J Cerebr Blood F Met **38**, 719–726 (2017).

[34] J Tithof, D H Kelley, H Mestre, Maiken Nedergaard, and John H Thomas, "Hydraulic resistance of periarterial spaces in the brain," Fluids and Barriers of the CNS **16**, 19 (2019).

[35] Piotr Hadaczek, Yoji Yamashita, Hanna Mirek, Laszlo Tamas, Martha C Bohn, Charles Noble, John W Park, and Krystof Bankiewicz, "The "Perivascular Pump" Driven by Arterial Pulsation Is a Powerful Mechanism for the Distribution of Therapeutic Molecules within the Brain," Mol. Ther. **14**, 69–78 (2006).

[36] J J Iliff, M Wang, D M Zeppenfeld, A Venkataraman, B A Plog, Yang Liao, R Deane, and M Nedergaard, "Cerebral Arterial Pulsation Drives Paravascular CSF-Interstitial Fluid Exchange in the Murine Brain," J Neurosci **33**, 18190–18199 (2013).

[37] Kristian Nygaard Mortensen, Simon Sanggaard, H Mestre, Hedok Lee, Serhii Kostrikov, Anna L R Xavier, Albert Gjedde, Helene Benveniste, and Maiken Nedergaard, "Impaired Glymphatic Transport in Spontaneously Hypertensive Rats," J Neurosci **39**, 6365–6377 (2019).

[38] Ravi Teja Kedarasetti, Patrick J Drew, and Francesco Costanzo, "Arterial pulsations drive oscillatory flow of CSF but not directional pumping," Sci. Rep. , 1–12 (2020).

[39] Lynne E Bilston, David F Fletcher, Andrew R Brodbelt, and Marcus A Stoodley, "Arterial Pulsation-driven Cerebrospinal Fluid Flow in the Perivascular Space: A Computational Model," Computer Methods in Biomechanics and Biomedical Engineering **6**, 235–241 (2003).

[40] Mahdi Asgari, Diane de Zélicourt, and Vartan Kurtcuoglu, "Glymphatic solute transport does not require bulk flow," Sci. Rep. , 1–11 (2016).

[41] D Schley, R Carare-Nnadi, C P Please, V H Perry, and R O Weller, "Mechanisms to explain the reverse perivascular transport of solutes out of the brain," J. Theor. Biol. **238**, 962–974 (2006).

[42] Peng Wang and William L Olbricht, "Fluid mechanics in the perivascular space," J. Theor. Biol. **274**, 52–57 (2011).

[43] Alex J Smith, Xiaoming Yao, James A Dix, Byung-Ju Jin, and Alan S Verkman, "Test of the'glymphatic'hypothesis demonstrates diffusive and aquaporin-4-independent solute transport in rodent brain parenchyma," Elife **6**, e27679 (2017).

[44] Alex J. Smith and Alan S. Verkman, "The "glymphatic" mechanism for solute clearance in alzheimer's disease: game changer or unproven speculation?" The FASEB Journal **32**, 543–551 (2018), https://faseb.onlinelibrary.wiley.com/doi/pdf/10.1096/fj.201700999.

[45] Matteo Croci, Vegard Vinje, and Marie E Rognes, "Uncertainty quantification of parenchymal tracer distribution using random diffusion and convective velocity fields," Fluids and Barriers of the CNS , 1–21 (2019).

[46] M Keith Sharp, Roxana O Carare, and Bryn A Martin, "Dispersion in porous media in oscillatory flow between flat plates: applications to intrathecal, periarterial and paraarterial solute transport in the central nervous system," Fluids and Barriers of the CNS , 1–17 (2019).

[47] Susanne J van Veluw, Steven S Hou, Maria Calvo-Rodriguez, Michal Arbel-Ornath, Austin C Snyder, Matthew P Frosch, Steven M Greenberg, and Brian J Bacskai, "Vasomotion as a Driving Force for Paravascular Clearance in the Awake Mouse Brain," Neuron , 1–31 (2019).

[48] Vegard Vinje, Anders Eklund, Kent-André Mardal, Marie E Rognes, and Karen-Helene Støverud, "Intracranial pressure elevation alters CSF clearance pathways," Fluids and Barriers of the CNS , 1–19 (2020).

[49] Mohammad M Faghih and M Keith Sharp, "Mechanisms of tracer transport in cerebral perivascular spaces," Journal of Biomechanics **118**, 110278 (2021).

[50] Aditya Raghunandan, Antonio Ladron-de Guevara, J Tithof, H Mestre, Ting Du, Maiken Nedergaard, John H Thomas, and D H Kelley, "Bulk flow of cerebrospinal fluid observed in periarterial spaces is not an artifact of injection," Elife **10**, e65958 (2021).

[51] Antonio Ladrón-de Guevara, Jessica K. Shang, Maiken Nedergaard, and Douglas H. Kelley, "Perivascular pumping in the mouse brain: Realistic boundary conditions reconcile theory, simulation, and experiment," bioRxiv (2020), 10.1101/2020.07.02.183608,

https://www.biorxiv.org/content/early/2020/07/02/2020.07.02.183608.full.pdf.

[52] T D Nevins and D H Kelley, "Front tracking for quantifying advection-reaction-diffusion," Chaos **27**, 043105–10 (2017).

[53] T D Nevins and D H Kelley, "Front tracking velocimetry in advection-reaction-diffusion systems," Chaos **28**, 043122–11 (2018).

[54] H Mestre, Ting Du, Amanda M Sweeney, Guojun Liu, Andrew J Samson, Weiguo Peng, Kristian Nygaard Mortensen, Frederik Filip Stæger, Peter A R Bork, Logan Bashford, Edna R Toro, J Tithof, D H Kelley, John H Thomas, Poul G Hjorth, Erik A Martens, Rupal I Mehta, Orestes Solis, Pablo Blinder, David Kleinfeld, Hajime Hirase, Yuki Mori, and Maiken Nedergaard, "Cerebrospinal fluid influx drives acute ischemic tissue swelling," Science **9**, eaax7171–24 (2020).

[55] Mohammad M Faghih and M Keith Sharp, "Is bulk flow plausible in perivascular, paravascular and paravenous channels?" Fluids and Barriers of the CNS , 1–10 (2018).

[56] Julian Rey and Malisa Sarntinoranont, "Pulsatile flow drivers in brain parenchyma and perivascular spaces: a resistance network model study," Fluids and Barriers of the CNS **15**, 20 (2018).

[57] Pablo Blinder, Philbert S Tsai, John P Kaufhold, Per M Knutsen, Harry Suhl, and David Kleinfeld, "The cortical angiome: an interconnected vascular network with noncolumnar patterns of blood flow," Nat Neurosci **16**, 889 EP – (2013).

[58] Qiaoli Ma, Benjamin V Ineichen, Michael Detmar, and Steven T Proulx, "Outflow of cerebrospinal fluid is predominantly through lymphatic vessels and is reduced in aged mice," Nat. Commun. , 1–13 (2017).

[59] Qiaoli Ma, Yann Decker, Andreas Müller, Benjamin V Ineichen, and Steven T Proulx, "Clearance of cerebrospinal fluid from the sacral spine through lymphatic vessels," J Exp Med **82**, jem.20190351–11 (2019).

[60] N E Fultz, G Bonmassar, K Setsompop, R A Stickgold, B R Rosen, J R Polimeni, and L D Lewis, "Coupled electrophysiological, hemodynamic, and cerebrospinal fluid oscillations in human sleep," Science (2019).

[61] Sunil Koundal, Rena Elkin, Saad Nadeem, Yuechuan Xue, Stefan Constantinou, Simon Sanggaard, Xiaodan Liu, Brittany Monte, Feng Xu, William Nostrand, Maiken Nedergaard, Hedok Lee, Joanna Wardlaw, Helene Benveniste, and Allen Tannenbaum, "Optimal Mass Transport

with Lagrangian Workflow Reveals Advective and Diffusion Driven Solute Transport in the Glymphatic System," Sci. Rep. , 1–18 (2020).

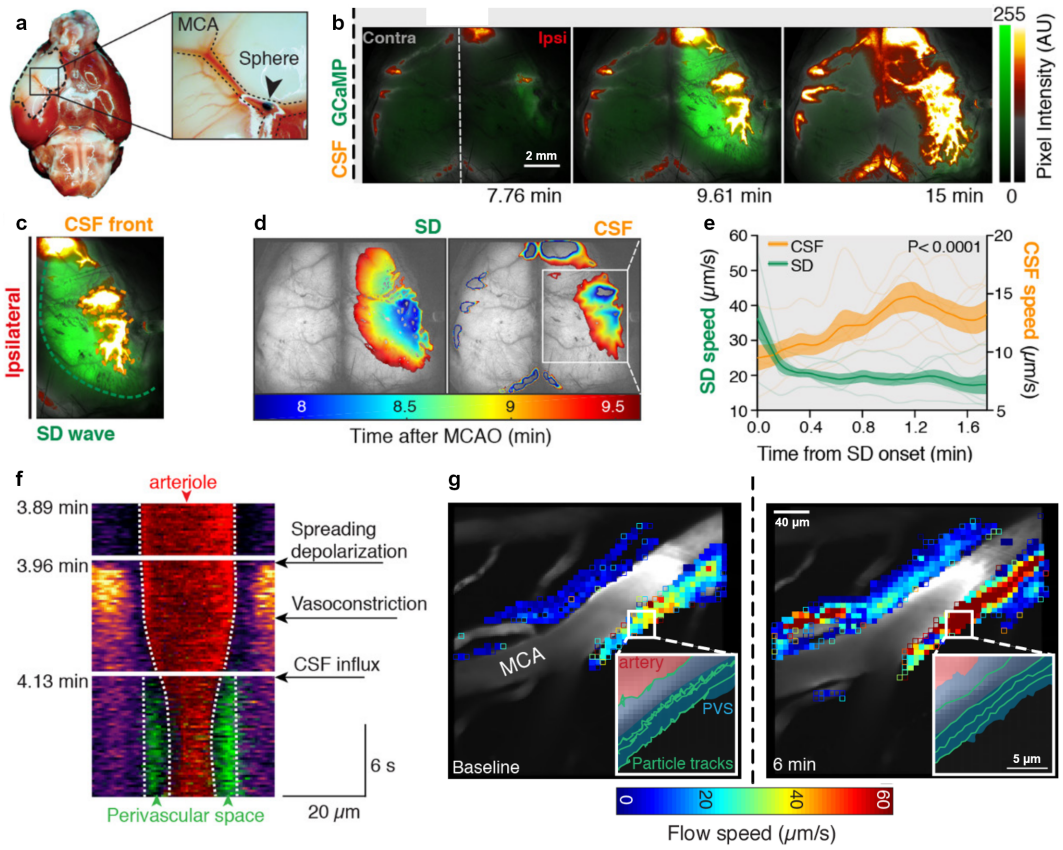

FIG. 9. Swelling soon after stroke is due primarily to cerebrospinal fluid flow. (a) We injected 1 mm spheres to induce stroke in mice by obstructing the middle cerebral artery (MCA). (b) Transcranial imaging shows that cerebrospinal fluid (marked with dye, shown red-orange) rushes into the brain following following a spreading depolarization wave of neural activity (green), primarily in the ipsilateral hemisphere (where the sphere was injected), not in the contralateral hemisphere. (c) We located fronts separating bright from dim regions, for both dye in CSF and spreading depolarization (SD). (d) Tracking fronts showed that CSF inflow lags depolarization. (e) Tracking also showed that CSF accelerated after the depolarization propagated. (f) After depolarization, arterioles constrict, enlarging the surrounding perivascular space, which is then filled with CSF. Here, dextran dye (shown red) was injected intravenously to mark the arteriole, BSA-647 dye (shown green) was injected into the cisterna magna to mark the CSF, and neural activity (shown purple to yellow) was also visible in these genetically modified mice. (g) Particle tracking in surface PVSs shows pulsatile flow before artery obstruction, but smooth flow after, likely because flow during stroke is driven not by artery pulsation but by constriction. Adapted from [54].

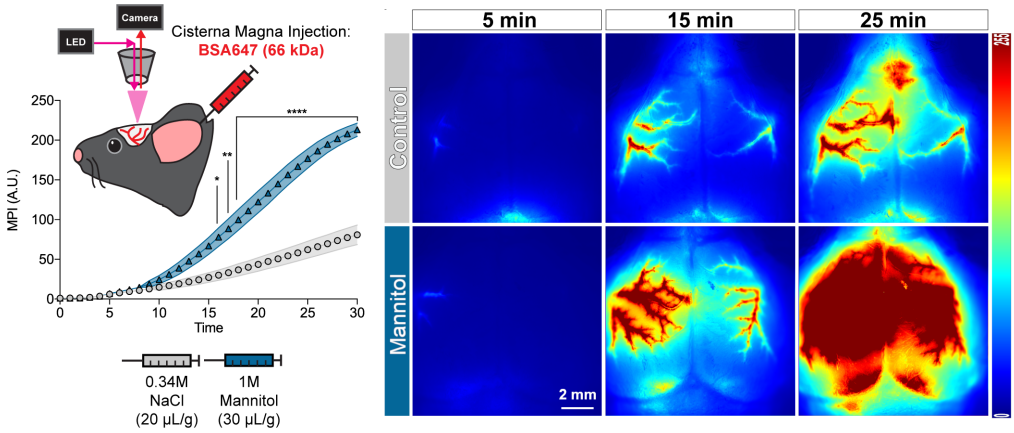

FIG. 10. Osmotic promotion of glymphatic flow might help deliver drugs to the brain. We injected dye into the cisterna magna and also injected either osmotically-neutral NaCl solution or concentrated mannitol solution. Dye entered brain tissue (increasing the mean pixel intensity, MPI) much more quickly in experiments using mannitol, as transcranial imaging shows. Adapted from [25].